Active microrheology of driven granular particles

Ting Wang,[1] Matthias Grob,[2] Annette Zippelius,[2,3] and Matthias Sperl[1]
[1]*Institut für Materialphysik im Weltraum, Deutsches Zentrum für Luft und Raumfahrt (DLR), 51170 Köln, Germany*
[2]*Georg-August-Universität Göttingen, Institut für Theoretische Physik, Friedrich-Hund-Platz 1, 37077 Göttingen, Germany*
[3]*Max-Planck-Institut für Dynamik und Selbstorganisation, Am Faßberg 17, 37077 Göttingen, Germany*
(Received 23 December 2013; published 28 April 2014)

When pulling a particle in a driven granular fluid with constant force F_{ex}, the probe particle approaches a steady-state average velocity v. This velocity and the corresponding friction coefficient of the probe $\zeta = F_{ex}/v$ are obtained within a schematic model of mode-coupling theory and compared to results from event-driven simulations. For small and moderate drag forces, the model describes the simulation results successfully for both the linear as well as the nonlinear region: The linear response regime (constant friction) for small drag forces is followed by shear thinning (decreasing friction) for moderate forces. For large forces, the model demonstrates a subsequent increasing friction in qualitative agreement with the data. The square-root increase of the friction with force found in [Fiege *et al.*, Granul. Matter **14**, 247 (2012)] is explained by a simple kinetic theory.

DOI: 10.1103/PhysRevE.89.042209 PACS number(s): 45.70.−n, 82.70.Dd, 83.60.Df, 83.10.Gr

I. INTRODUCTION

Active microrheology (AM) studies the mechanical response of a many-particle system on the microscopic level by pulling individual particles through the system either with constant force or at constant velocity [1]. While in passive microrheology only the linear response can be probed, AM can also be applied to explore the nonlinear response by imposing large drag forces. An external force F_{ex} can be imposed by magnetic [2] or optical tweezers [3] to a probe particle embedded in a soft material and then the corresponding steady-state velocity $\langle v\rangle$ is measured by optical microscopy [4]. Recently, AM experiments [2] and simulations [5–7] for dense colloidal suspensions found that (i) in the linear-response region, the friction coefficient of the probe $\zeta = F_{ex}/\langle v\rangle$ directly indicates the increasing rigidity of the system when approaching the glass transition from the liquid state; (ii) in the nonlinear response region, the friction coefficient tends to decrease to a certain value with increasing pulling force—an effect reminiscent of shear thinning in macrorheology. Both effects could be explained by an extension of mode-coupling theory (MCT) to describe AM [8,9].

Within the MCT interpretation, the description of AM for colloidal suspensions is based on the existence of a glass transition in such systems. The interplay between growing density correlations by glass formation and the suppression of those correlations by microscopic shear explains the observed behavior of the friction microscopically. In addition to colloidal suspensions, a glass transition is also predicted by MCT for driven granular systems [10–12]. Here, the energy lost in the dissipative interparticle collisions is balanced by random agitation. Starting from the nonequilibrium steady state of this homogeneously driven granular system, the corresponding AM shall be elaborated below.

In AM of granular matter similar phenomena as in colloidal suspensions are found: (i) Dramatic increasing of the friction coefficient and (ii) shear thinning have been identified in experiments with horizontally vibrated granular particles [13,14], and both effects were reproduced in recent simulations of a two-dimensional granular system [15]. Moreover, for large pulling forces in the simulation, beyond the thinning regime the friction coefficients increase again and exhibit power-law behavior close to a square root: $\zeta(F_{ex}) \propto \sqrt{F_{ex}}$ for $F_{ex} \gg 1$. This finding is in contrast to the predicted constant friction (second linear regime) in the colloidal hard-sphere system [8,9]. In the following, we shall demonstrate how a schematic MCT model can capture the increase with friction for large forces. In addition, for dilute systems we shall derive a square-root law for large forces exactly.

II. DYNAMICS OF A GRANULAR INTRUDER

The driven granular system under consideration is composed of N identical particles interacting with each other. One probe particle experiences a constant pulling force $\boldsymbol{F}_{ex}$. The dynamics of the system is given for every particle i by the equation of motion

$$m\dot{\boldsymbol{v}}_i = -\zeta_0 \boldsymbol{v}_i + \boldsymbol{f}^i_{\rm int} + \boldsymbol{\eta}_i + \boldsymbol{F}_{ex}\delta_{i,s}, \tag{1}$$

where ζ_0 is the bare friction depending on the friction of the surrounding medium, which for large values is reminiscent of a colloidal suspension. The force $\boldsymbol{f}^i_{\rm int}$ is the particle interaction force, which for the granular case is typically given by a collision rule to include the energy loss at contact. $\boldsymbol{\eta}_i$ is a random driving force satisfying a fluctuation dissipation relation $\langle \boldsymbol{\eta}_i(t)\boldsymbol{\eta}_j(t')\rangle = 2\zeta_0 k_B T/m\delta_{i,j}\delta(t-t')$, and the constant pulling force $\boldsymbol{F}_{ex}$ is imposed on the probe particle (denoted s) only. Models similar to Eq. (1) have been proposed frequently and elaborated on regarding their dynamics in the description of driven granular systems [16].

A. Schematic model

The use of MCT for the description of glassy dynamics can be found fully self-contained and in considerable detail in recent reviews and books such as Ref. [18]. We shall outline briefly the general framework of the theory as follows. MCT describes the dynamics in the liquid state by correlation functions for which one can derive the microscopic equations of motion for the system under consideration. Using projection-operator formalisms, the equations of motion can be reformulated exactly as integrodifferential equations for

 ©2014 American Physical Society

the correlation functions where the integral terms represent memory effects. To close the equations, an approximation—the mode-coupling factorization—is invoked, and the resulting equations are solved numerically by asymptotic expansion. In addition to the full microscopic MCT equations, simplified so-called schematic models can be used that capture the mathematical structure of the full theory but are easier to solve [18]. The MCT formalism has been extended to dissipative granular dynamics in Ref. [12]. The theory predicts a glass transition for a driven granular fluid for all degrees of inelasticity, parametrized by the coefficient of resitution ε. Hence, there is a glass transition line in the phase diagram spanned by volume fraction and ε. In the following, we build on these results to discuss the dynamics of a single intruder pulled through a dissipative granular medium. As a first step toward a full MCT theory, we generalize schematic models that have been devised for the dynamics of an intruder in a colloidal fluid [9] to the case of an intruder inside a dissipative granular host fluid.

The friction coefficient of the probe can be calculated by the integration-through-transients (ITT) method combined with the MCT approximation. This procedure was first applied to describe the macrorheology [17] and was later extended to AM for colloidal suspension [8,9]. We follow the approach in Refs. [8,9] to construct a schematic MCT model for driven granular systems. Different from colloidal systems, the equations of motion for the density autocorrelation functions for both the bulk system and the probe particle, $\phi_{\boldsymbol{q}}(t) := \langle \rho_{\boldsymbol{q}}(t)\rho^*_{\boldsymbol{q}}\rangle/\langle \rho_{\boldsymbol{q}}\rho^*_{\boldsymbol{q}}\rangle$ and $\phi^s_q(t) := \langle \exp\{i\boldsymbol{q}\cdot[\boldsymbol{r}_s(t)-\boldsymbol{r}_s]\}\rangle$, respectively, include a second time derivative, because granular systems are not overdamped. Here, $\langle\cdots\rangle$ denotes the ensemble average and $\rho_{\boldsymbol{q}}(t) := \sum_{i=1}^{N} e^{i\boldsymbol{q}\cdot\boldsymbol{r}(t)}$ is the Fourier transform of the density. In schematic models the dependence of the correlation functions on the wave vector $\boldsymbol{q}$ is ignored. Instead, the correlation functions are evaluated at one particular wavenumber q_0, e.g., the maximum of the structure factor. The equations for $\phi(t) = \phi_{q_0}(t)$ and $\phi_s(t) = \phi^s_{q_0}(t)$ read

$$\begin{aligned}\ddot{\phi}(t) + \nu\dot{\phi}(t) + \Omega^2\left[\phi(t) + \int_0^t d\tau\, m(t-\tau)\dot{\phi}(\tau)\right] = 0\\ \ddot{\phi}_s(t) + \nu_s\dot{\phi}_s(t) + \Omega_s^2\left[\phi_s(t) + \int_0^t d\tau\, m_s(t-\tau)\dot{\phi}_s(\tau)\right] = 0.\end{aligned} \tag{2}$$

The first 3 terms in Eq. (2) describe oscillations with frequency $\Omega(\Omega_s)$, which are damped with rate $\nu(\nu_s)$. The last terms account for memory effects. In a schematic MCT model (called F_{12} model) the memory kernels are approximated by nonlinear functions of the correlation functions as follows:

$$\begin{aligned} m(t) &= v_1\phi(t) + v_2\phi^2(t)\\ m_s(t) &= v_A\phi(t)\mathrm{Re}[\phi_s(t)].\end{aligned} \tag{3}$$

The host fluid is assumed to be large enough so that its density correlation function is not affected by the external pulling force F_{ex}. Consequently, the collective dynamics is completely decoupled in Eqs. (2) and (3). Here, we are interested in the long-time behavior of $\phi(t)$, which is not affected by ν and Ω, so that we take $\nu = \Omega = 1$ for simplicity. The control parameters (v_1, v_2) of the host fluid determine the liquid or glassy state together with the distance of a chosen state point from a glass-transition line, which in the case of schematic models can be calculated analytically [18]. The state points $(v_1, v_2) = [v_1^c(1+\sigma), v_2^c(1+\sigma)]$ are specified by a distance σ to the transition line given by $v_1^c = v_2^c(2/\sqrt{v_2^c} - 1)$ with the specific choice $v_2^c = 2$ for the transition point.

The coupling strength between the probe and the host system is indicated by v_A. Ω_s^2 is the effective frequency of the correlation function of the probe and set to be $\Omega_s^2 = 1 - iF_{\mathrm{ex}}$. This result can be obtained exactly from Eq. (1) by considering the limit of vanishing interacting force:

$$\begin{aligned}\phi^s_{\boldsymbol{q}}(t) &= \exp\left(-\Omega^2_{s,\boldsymbol{q}}t^2\right)\\ \Omega^2_{s,\boldsymbol{q}} &= \frac{\boldsymbol{q}}{m}\cdot(\boldsymbol{q}k_BT - i\boldsymbol{F}_{\mathrm{ex}}) \to \frac{q_0^2}{m}k_BT\left(1 - i\frac{F_{\mathrm{ex}}}{q_0k_BT}\right).\end{aligned} \tag{4}$$

ν_s describes the dynamics of the density correlator of the probe for short time scales. In order to assure that $|\phi_s(t)| \leqslant 1$, it is required that

$$\nu_s > F_{\mathrm{ex}}, \tag{5}$$

which is obtained by solving the second equation in Eqs. (2) without the memory kernel. By integration of the density autocorrelators [8,9], we get the expression for the effective friction of the probe as

$$\zeta/\zeta_0 = 1 + \frac{q_0^2}{\zeta_0}k_BT\int_0^\infty dt\,\mathrm{Re}[\phi_s(t)]\phi(t). \tag{6}$$

Equation (5) shows clearly that ν_s depends on the pulling force. However, its dependence beyond the inequality can only be obtained from a microscopic theory. Within the schematic model, we have investigated several functional forms of $\nu_s(F_{\mathrm{ex}})$ complying with the constraint in Eq. (5). The simplest choice is the straightforward generalization of the colloidal case: (a) $\nu_s = 1 + F_{\mathrm{ex}}$. As shown below, this choice is not compatible with the data from simulations. This has led us to consider case (b) $\nu_s = 1 + F_{\mathrm{ex}}^2$. Ultimately, a microscopic derivation needs to show if case (b) can be obtained from the microscopic equations of motion, cf. [9].

The respective numerical solutions for the force-dependent friction coefficients are given in Fig. 1, where σ indicates the distance from the glass transition. The force-dependent friction of the probe exhibits three characteristic regimes. For small pulling forces in both models, the friction coefficient is constant, or equivalently, the average velocity of the probe is proportional to the external pulling force. This region extends to external forces of order unity and describes a linear response. When approaching the glass transition, the friction increases drastically as the correlation functions in Eq. (6) extend to increasingly longer time scales. Starting around $F_{\mathrm{ex}} \approx 1$, the linear-response regime ends and gives rise to shear thinning: The friction decreases and it is proportionally easier to pull the particle. Equivalently, the average velocity of the intruder increases faster than linear with external force. For the model in the left panel of Fig. 1, the friction ζ approaches the limiting value given by the bare friction ζ_0 and remains there for yet higher forces. This model hence describes behavior similar to the colloidal results for Newtonian microscopic dynamics. For the model in the right panel of Fig. 1, the friction approaches a minimum around $F_{\mathrm{ex}} \approx 100$ and starts increasing for higher pulling forces.

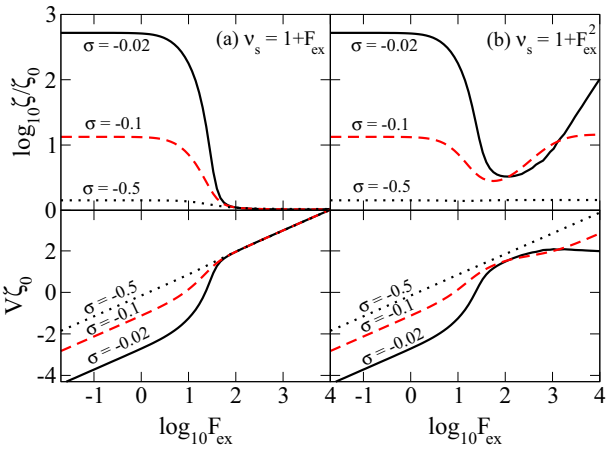

FIG. 1. (Color online) Force-dependent friction coefficient (upper panels) for different models of the damping $\nu_s(F_{\rm ex})$ together with the steady-state velocities (lower panels). σ specifies the distance from the glass-transition point in the schematic model.

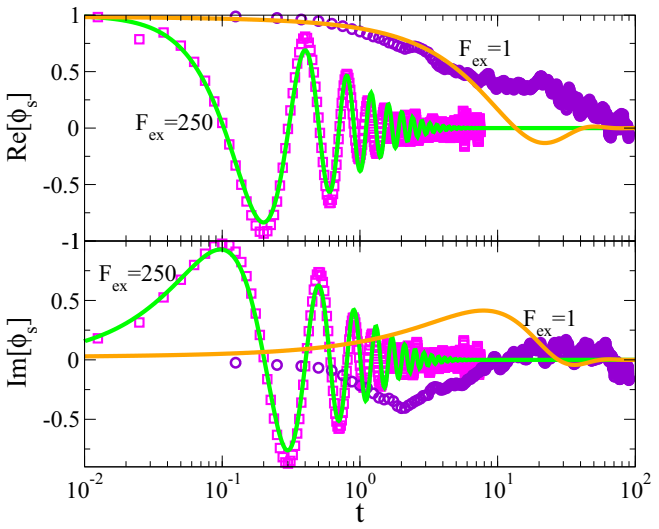

FIG. 2. (Color online) Comparison between the schematic model and the simulation data for the density autocorrelator of the probe particle at fixed packing fraction $\varphi = 0.8$ and energy dissipation $\varepsilon = 0.9$. The pulling forces are $F_{\rm ex} = 1$ and 250. The symbols represent the simulation data; the solid lines are the descriptions by the schematic model.

In comparison, the models in Figs. 1(a) and 1(b) are almost equivalent in the linear-response and shear-thinning regimes, where the friction in Eq. (6) is dominated by the memory effects leading to a slowing down of the relaxation. The difference in the microscopic damping ν_s does not play a significant role. In contrast, for large pulling forces, the correlation function $\phi_s(t)$ relaxes to zero rapidly and the integral Eq. (6) is dominated by the short-time part of the correlation functions.

B. Comparison with simulation data

The simulation is performed in two dimensions and the setup is the same as described in Ref. [15]: In a bidisperse mixture of hard disks with size ratio $R_s/R_b = 4/5$ of small to big particles and a respective mass ratio $m_s/m_b = 16/25$, an intruder of radius $R_0 = 2R_s$ and mass $m_0 = 4m_s$ is suspended. All collisions are inelastic, characterized by the coefficient of restitution, ε. The particles are kicked randomly to balance energy input and dissipation by drag and inelastic collisions. Lengths and masses are measured such that $R_s = 1$ and $m_s = 1$ and a time scale is set by requiring that the granular temperature $T_G = 1$ in the system with $F_{\rm ex} = 0$. An event driven code is implemented to simulate $N = 10^4$ particles for a wide range of $F_{\rm ex}$ and ε.

We adopt with $\nu_s = 1 + F_{\rm ex}^2$ the second schematic model to compare with the simulation data in detail. Since the schematic models only capture the overall mathematical structure of the theory, it is equally well applicable in both three and two dimensions as the underlying glass transitions are similar in both 2D and 3D [12]. The same holds for monodisperse and bidisperse systems.

Figure 2 shows the fit of the measured correlation functions by the model. The numerical solution of the density autocorrelator of the intruder fits quite well the corresponding simulation data for the moderately high force $F_{\rm ex} = 250$. For the smaller force $F_{\rm ex} = 1$, it shows some deviations. The fitting parameters are $v_A = 200$, $\sigma = -0.05$ for $\varepsilon = 0.9$ as well as (not shown in Fig. 2) $v_A = 300$, $\sigma = -0.09$ for $\varepsilon = 0.7$ and $v_A = 600$, $\sigma = -0.13$ for $\varepsilon = 0.1$. The other parameters are the same as the ones mentioned above.

The corresponding fit of the friction coefficients is given in Fig. 3. In the regime of small forces, the schematic model shows a linear-response plateau. The simulation data also show a plateau for small forces (see Fig. 3 in Ref. [15]). As the glass transition is approached, this regime moves to smaller forces, so that it is visible in Fig. 3 only for the smallest $\varepsilon = 0.1$, which is further away from the glass transition than $\varepsilon = 0.9$ and 0.7. However, for $\varepsilon = 0.1$ and $\varphi = 0.8$ the simulations become increasingly difficult for small forces due to the occurrence of long-lasting contacts. Hence, the error bars become comparable to the result itself. For large pulling forces,

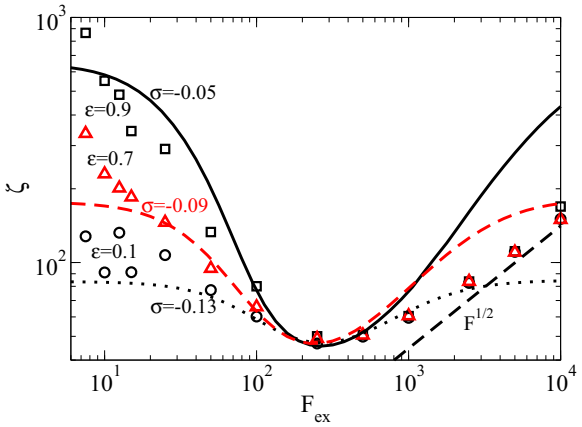

FIG. 3. (Color online) Effective friction of the intruder for different energy dissipation $\varepsilon = 0.9$, 0.7, and 0.1 at fixed packing fraction $\varphi = 0.8$ of the host fluid. Individual data points show the simulation results; curves represent the results from the schematic models. The dashed straight line indicates the slope of $\sqrt{F}$.

the model shows qualitatively how the increasing friction coefficient can be rationalized within a schematic model. While the schematic model exhibits different limits for varying distances from the glass transition, the simulation data follow the same curve for $F_{ex} \gtrsim 500$. Between the extreme regimes of large and small pulling forces the friction coefficient exhibits a minimum that is similar for all distances from the glass transition for both the schematic model and the simulation.

While the schematic model may only qualitatively fit the simulation data for the friction coefficient in Fig. 3, in addition to the good agreement of the correlation functions in Fig. 2, the results are also consistent with the predictions from MCT for hard spheres [10–12]. For smaller dissipation, i.e., larger coefficient of restitution ε in Fig. 3, the data can be described only by choosing points closer to the glass-transition line in the schematic model. Smaller distances to the glass transition given by smaller values of σ indicate that for the same density of $\varphi = 0.8$ the data for $\varepsilon = 0.9$ are much closer to the glass transition than for $\varepsilon = 0.1$ with $\varepsilon = 0.7$ located in between. This finding is in agreement with the predicted increase of the glass-transition density with decreasing ε within MCT [10–12].

III. KINETIC THEORY IN THE LOW-DENSITY LIMIT

To clarify the origin of the scaling law $\zeta \propto \sqrt{F_{ex}}$ in the large-force asymptote, we propose a simple kinetic theory in the following. The simulation result from Ref. [15] has shown that the scaling law is independent of packing fraction. Therefore, a potential explanation of the increased friction by jamming or shear thickening seems unlikely. Also, the correlation functions for large pulling forces decay relatively quickly, cf. Fig. 2, also contradicting a buildup of long-time glass-like contributions to the integrals like in Eq. (6). In the following we shall therefore focus on the low-density limit, where exact solutions can be obtained.

The formal solution of $\boldsymbol{v}(t)$ in Eq. (1) can be readily obtained and the corresponding ensemble average of the velocity of the intruder is given by

$$\langle \boldsymbol{v}(t) \rangle = \frac{\boldsymbol{F}_{ex}}{\zeta_0}\left(1 - e^{-\frac{\zeta_0}{m}t}\right) + \frac{e^{-\frac{\zeta_0}{m}t}}{m}\int_0^t e^{\frac{\zeta_0}{m}t'} \langle \boldsymbol{f}_{int}(t') \rangle dt', \qquad (7)$$

where we have averaged out the initial velocity and the random force: $\langle \boldsymbol{v}_0 \rangle = 0$ and $\langle \boldsymbol{\eta}(t) \rangle = 0$.

The direct calculation of $\langle \boldsymbol{f}_{int}(t) \rangle$ in Eq. (7) is difficult. The key point of our kinetic theory is to introduce the mean free path of the intruder, $l_0 = \rho^{-1}\sigma_{cr}$, where $\rho = N/V$ is the particle number density and σ_{cr} is the intruder's cross section, which for hard sphere reduces to $\sigma_{cr} = 4\pi R^2$. Let us denote the collision time as t_c. Between two successive collisions $nt_c < t < (n+1)t_c$, there is no interaction force in the hard sphere limit, $\langle \boldsymbol{f}_{int}(t) \rangle = 0$. On average, after t_c a collision event causes a momentum transfer from the intruder to its collision partner of the order of the intruder's complete momentum. The velocity of the intruder increases again from almost zero due to the constant pulling force. Statistically, the intruder's velocity exhibits periodic motion. Consider the motion of the probe in the first period: The average velocity reads

$$\langle \boldsymbol{v}(t) \rangle = \frac{\boldsymbol{F}_{ex}}{\zeta_0}\left(1 - e^{-\frac{\zeta_0}{m}t}\right), \quad 0 \leqslant t \leqslant t_c, \qquad (8)$$

and the displacement of the motion satisfies

$$l_0 = \left| \int_0^{t_c} \langle \boldsymbol{v}(t) \rangle dt \right| = \frac{F_{ex}}{\zeta_0}\left[t_c - \frac{m}{\zeta_0}\left(1 - e^{-\frac{\zeta_0}{m}t_c}\right)\right]. \qquad (9)$$

The average velocity of the probe is given by

$$\langle v_s \rangle = \frac{1}{t_c}\left| \int_0^{t_c} \langle \boldsymbol{v}(t) \rangle dt \right| = \frac{l_0}{t_c}. \qquad (10)$$

In general, the friction of the probe $\langle v_s \rangle$ can be calculated by Eqs. (9) and (10) exactly. We first consider the two limiting cases $t_c \gg \frac{m}{\zeta_0}$ (overdamped limit) and $t_c \ll \frac{m}{\zeta_0}$ (ballistic regime).

In the overdamped limit, velocity relaxation dominates over collisions and the collision times are large,

$$t_c = \frac{l_0\zeta_0}{F_{ex}} \gg \frac{m}{\zeta_0} \qquad (11)$$

or equivalently,

$$\frac{F_{ex}}{\zeta_0^2} \ll \frac{l_0}{m}. \qquad (12)$$

The average velocity and the friction of the intruder can be obtained by Eq. (10) and definition of the friction itself, yielding

$$\langle v_s \rangle = F_{ex}/\zeta_0, \quad \zeta = \zeta_0. \qquad (13)$$

The friction experienced by the intruder is dominated by the effective friction originating from the medium.

In the ballistic limit, collisions dominate over velocity relaxation. Expanding $e^{-\frac{\zeta_0}{m}t}$ in Eq. (9) to second order, we get

$$t_c = \sqrt{\frac{2ml_0}{F_{ex}}} \ll \frac{m}{\zeta_0}. \qquad (14)$$

The ballistic limit is given by the presence of pulling forces very large compared to the bare friction,

$$\frac{F_{ex}}{\zeta_0^2} \gg \frac{2l_0}{m}. \qquad (15)$$

The average velocity and the friction of the probe are

$$\langle v_s \rangle = \sqrt{\frac{l_0 F_{ex}}{2m}} \propto \sqrt{F_{ex}}$$
$$\zeta = \sqrt{\frac{2m F_{ex}}{l_0}} \propto \sqrt{F_{ex}}. \qquad (16)$$

Both the velocity as well as the friction are proportional to the square-root of the external pulling force and independent of the bare friction.

The general solution of Eqs. (9) and (10) can be calculated in parametric form and is given in Fig. 4, where the crossover is shown for the friction coefficient from a constant (linear large-force behavior of the velocity) to the square-root increase (square-root increase of the velocity for large forces). The

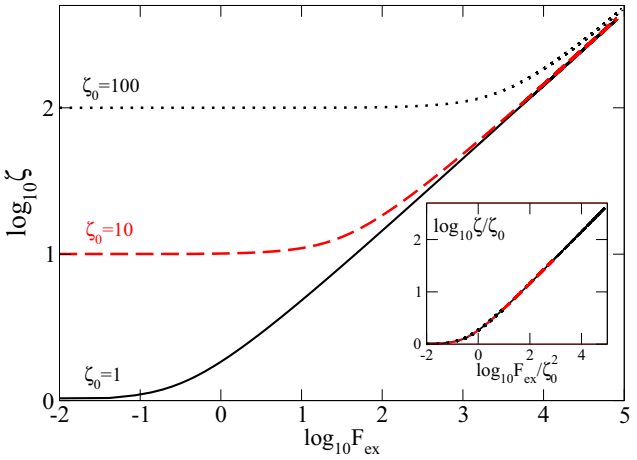

FIG. 4. (Color online) Force-friction relation at large forces for different damping in the low-density limit.

reason why for a driven granular system the friction of the probe increases as $\zeta \propto \sqrt{F_{\rm ex}}$ in the large-force regime, but for colloidal hard-sphere systems the friction only decreases to a constant value, can be explained as follows. For different bare frictions ζ_0, the $F_{\rm ex}$-ζ plots can be rescaled as $F_{\rm ex}/\zeta_0^2$ versus ζ/ζ_0, cf. the inset in Fig. 4. The behavior of the probe in the large-pulling-force regime is determined by the ratio of the collision time scale over the Brownian velocity relaxation time scale, $t_c/\frac{m}{\zeta_0}$, or equivalently the value of the rescaled force $F_{\rm ex}m/(\zeta_0^2 l_0)$. In a driven granular system, the bare friction is quite small compared with the one in a Brownian suspension, $\zeta_0 = 1$ in the granular simulation [15] and $\zeta_0 = 50$ in the colloidal one [5]. Indeed, one would also obtain the same asymptotic behavior $\zeta \propto \sqrt{F_{\rm ex}}$ for Brownian systems for extremely large pulling forces.

IV. CONCLUSION

We have investigated the microrheology of the driven granular hard-sphere system by a schematic model and a simple kinetic theory. For small and moderate external pulling forces, the schematic model agrees reasonably well with the simulation data, cf. Fig. 3, and implies that the glass-transition density increases with smaller coefficient of restitution ε, confirming predictions from mode-coupling theory [10–12]. For large forces, glassy dynamics becomes irrelevant and a simple kinetic theory clarifies the origin of the scaling of the friction with increasing pulling force. When damping by a surrounding fluid dominates the motion of the intruder at high forces, a second linear regime emerges where the friction becomes constant. When collisions dominate, the friction increases in a square-root law, $\zeta \propto \sqrt{F_{\rm ex}}$. Such behavior of the drag force, $F_{\rm ex} \propto v^2$, is reminiscent of Bagnold's law for granular rheology where the shear stress is proportional to the square of the shear rate.

While the derivation of the equations above implies the existence of a thermostat to ensure a steady state at the presence of energy dissipation, one may argue that for high enough velocities of the intruder, sufficient energy may be injected into the host fluid to overcome the necessity of an additional thermostat: Consistent with that view, experiments without thermostat but high intruder velocities [19] found for high densities that the average drag force F increased quadratically with the pulling velocity v of the intruder, which is consistent with $\zeta \propto \sqrt{F_{\rm ex}}$ found above.

In the models presented in this work, the phenomenon of increasing friction ζ for high pulling forces is not specific to the details of granular dynamics; it may only be more likely to access that high-force regime in granular simulations and experiments for typical control parameters. The elaboration of the microscopic version of the theory similar to the Brownian case [9] shall clarify this issue in the future.

ACKNOWLEDGMENTS

We acknowledge support from DAAD and DFG within FOR1394. We thank Andrea Fiege, Matthias Fuchs, Till Kranz, Leo Silbert, Thomas Voigtmann, Anoosheh Yazdi, and Peidong Yu for valuable discussions.

[1] T. M. Squires and T. G. Mason, Annu. Rev. Fluid Mech. **42**, 413 (2010).
[2] P. Habdas, D. Schaar, A. C. Levitt, and E. R. Weeks, Europhys. Lett. **67**, 477 (2004).
[3] A. Meyer, A. Marshall, B. G. Bush, and E. M. Furst, J. Rheol. **50**, 77 (2006).
[4] J.-A. Conchello and J. W. Lichtman, Nat. Meth. **2**, 920 (2005).
[5] M. V. Gnann, I. Gazuz, A. M. Puertas, M. Fuchs, and T. Voigtmann, Soft Matter **7**, 1390 (2011).
[6] D. Winter, J. Horbach, P. Virnau, and K. Binder, Phys. Rev. Lett. **108**, 028303 (2012).
[7] D. Winter and J. Horbach, J. Chem. Phys. **138**, 12A512 (2013).
[8] I. Gazuz, A. M. Puertas, T. Voigtmann, and M. Fuchs, Phys. Rev. Lett. **102**, 248302 (2009).
[9] I. Gazuz and M. Fuchs, Phys. Rev. E **87**, 032304 (2013).
[10] W. T. Kranz, M. Sperl, and A. Zippelius, Phys. Rev. Lett. **104**, 225701 (2010).
[11] M. Sperl, W. T. Kranz, and A. Zippelius, Europhys. Lett. **98**, 28001 (2012).
[12] W. T. Kranz, M. Sperl, and A. Zippelius, Phys. Rev. E **87**, 022207 (2013).
[13] R. Candelier and O. Dauchot, Phys. Rev. Lett. **103**, 128001 (2009).
[14] R. Candelier and O. Dauchot, Phys. Rev. E **81**, 011304 (2010).
[15] A. Fiege, M. Grob, and A. Zippelius, Granular Matter **14**, 247 (2012).
[16] A. Puglisi, A. Baldassarri, and V. Loreto, Phys. Rev. E **66**, 061305 (2002).
[17] M. Fuchs and M. E. Cates, Phys. Rev. Lett. **89**, 248304 (2002).
[18] W. Götze, *Complex Dynamics of Glass-Forming Liquids—A Mode-Coupling Theory* (Oxford University Press, Oxford, 2009).
[19] Y. Takehara, S. Fujimoto, and K. Okumura, Europhys. Lett. **92**, 44003 (2010).